AIAA-93-0631
Corrections to Fringe Distortion due to Flow Density Gradients in Optical Interferometry

Y.C.Cho, NASA Ames Research Center, Moffett Field, CA;
L.W.Carr, U.S.Army ATCOM, NASA Ames Research Center, Moffett Field, CA; and
M.S.Chandrasekhara, Naval Postgraduate School, Monterey, CA

31st Aerospace Sciences Meeting & Exhibit
January 11-14, 1993 / Reno, NV

DISCLAIMER NOTICE

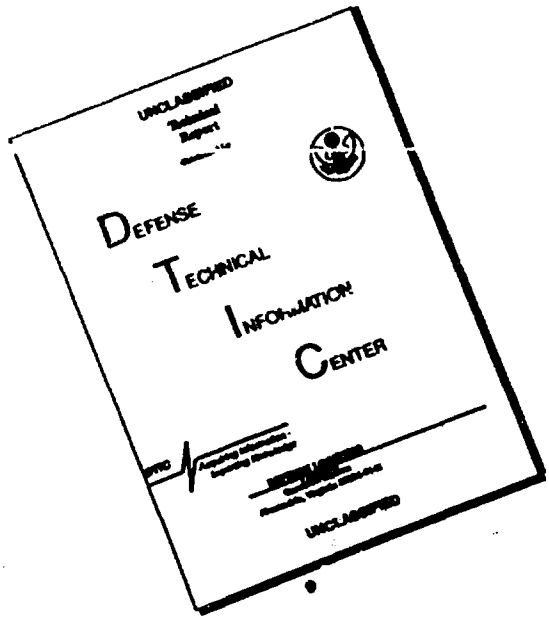

THIS DOCUMENT IS BEST QUALITY AVAILABLE. THE COPY FURNISHED TO DTIC CONTAINED A SIGNIFICANT NUMBER OF PAGES WHICH DO NOT REPRODUCE LEGIBLY.

Corrections to Fringe Distortion due to Flow Density Gradients in Optical Interferometry

Y. C. Cho[1]
Information Sciences Division
NASA Ames Research Center, Moffett Field, CA 94035-1000

L.W. Carr[2]
Aeroflightdynamics Directorate, U.S.Army ATCOM
and Fluid Mechanics Laboratory Branch
NASA Ames Research Center, Moffett Field, CA 94035-1000

M.S. Chandrasekhara[3]
Navy-NASA Joint Institute of Aeronautics
Department of Aeronautics and Astronautics
Naval Postgraduate School, Monterey, CA 93943

Abstract

An analytical method is formulated to account for distortions of optical interferograms used for studies of flow over airfoils experiencing dynamic stall. It is shown that such distortions are generated primarily due to optical path deflections in the test flow , caused by large density gradients. Such in-flow optical path deflections are neglected in conventional optical techniques for flow studies. The present method employs a ray analysis to determine these in-flow optical path deflections, and accurately predicts the interferogram distortions

Nomenclature

a	coefficient of y in expansion of air density as a function of, Eq. (11)
b	coefficient of y^2 in expansion of air density as a function of y, Eq.(11)
e	base of natural logarithms
f	focal length of spherical mirror, Fig. 3
I	light intensity
I_0	intensity of an incident light
K	Gladstone-Dale constant, Eq. (1)
L	wind tunnel span (25.4 cm), Fig. 2
ℓ	Thickness of glass window, Fig.2
M	Free stream Mach number
m	image magnification, Eq. (25)
n	(spatially varying) index of refraction of air
p	distance from mirror to an object plane, Fig. 3
q	distance from mirror to an image plane, Fig. 3
s	one-dimensional spatial coordinate variable along a ray
w	a parameter, Eq. (15)
x, y, z	spatial coordinates: x - mean flow direction, y - vertical, z - spanwise
y_0	y-coordinate of an incident ray at z=0
y_e	y-coordinate, Eq. (26) and Fig.4
y_L	y-coordinate of a ray at exit plane z=L
y'	tangential slope of a ray, Eq. (17)
y'_L	tangential slope of a ray at exit plane z=L
α	angle of attack of airfoil
β	$\sqrt{2Kb}$, Eq. 16
γ	$\Delta\rho/\rho_0$
δ	virtual displacement at an object plane, Eq. (22) and Figs. 2 and 3
δ_0	virtual displacement at z=0
δ_L	virtual displacement at z=L
$\bar{\delta}$	image displacement, Eq. (23)

[1] *Senior Research Scientist/Project Leader.*

[2] *Group Leader, Unsteady Viscous Flows; Member AIAA.*

[3] *Associate Director and Research Associate Professor; Assoc. Fellow AIAA.*

$\tilde{\delta}_0$	image displacement, focused on object plane z=0
$\tilde{\delta}_L$	image displacement, focused on object plane z=L
θ	angle of deflected ray measured from z-axis
ρ	(spatially varying) air density
ρ_0	ambient air density
ρ_s	air density at surface of airfoil
ρ_∞	air density in free stream
$\Delta\rho$	$\rho_\infty - \rho_s$

1. Background

A real-time optical interferometry technique has recently been used at NASA Ames Research Center to study dynamic stall over an oscillating airfoil in compressible flows.[1,2] During this investigation, a time sequence of interferograms was documented and analyzed. Each interferogram typically displays a fringe pattern delineating the density field surrounding the airfoil. The separation of two adjacent fringes corresponds to a phase increment of 2π. The fringe intensity varies sinusoidally along a line passing from one fringe to the next one, implying a linear change of the phase and of the flow density within the fringe separation. As the flow velocity increases, the fringe frequency increases locally in regions near the airfoil surface, indicating the presence of a large density gradient.

At high Mach numbers, the interferogram suffers distortions locally where the fringe frequency is very high. Evidence of such distortions is exhibited by fringes that separate from or penetrate into the image of the upper surface of the airfoil at angles of attack $\alpha = 5° \sim 15°$, and flow velocities $M = 0.3 \sim 0.45$, that is, when the airfoil is experiencing very high levels of lift [see Plate I]. Another example of the distortion is manifested near the leading edge of the airfoil for large flow velocities. In this case, the fringes disappear locally leaving the interferogram with a completely dark spot as shown in Plate II. Detailed understanding and correction of interferogram distortions is critical to accurate analysis of the compressible flow that occurs on airfoils at high angles of attack. Correction of these distortions is absolutely necessary if quantitative analysis of the flow is to be considered in this unsteady flow environment.

The primary cause of the observed fringe distortions is evidently optical refraction induced by the large density gradients. An optical refraction in a test flow may be regarded as composed of two elements: Phase modification and path deflection. Although the in-flow deflections are effected as modifications of the wave front defined as a surface of constant phase, it is neglected in conventional optical methods applied to flow studies such as shadowgraphs and schlieren systems. These methods assume that the deflection occurs only at the interface of the test flow and the surrounding medium. Even in optical interferometry, the in-flow deflections were previously neglected because their effects were insignificant or appeared to be insignificant. We initially took such neglect for granted, and suspected that a potential cause of the observed fringe distortions were the double refractions of the light at both surfaces of the exit glass window. However, an in-depth investigation, both analytical and experimental, showed that such double refractions would displace image planes but could not generate the observed image distortions. In this paper, an analytical method has been formulated to account for the interferogram distortions including in-flow optical path deflections which are determined by using a ray analysis.

2. Experimental Setup

In the present study, the airfoil is mounted in a wind tunnel between two 2.54 cm thick glass windows which are oriented perpendicular to the spanwise coordinate z-axis and parallel to each other. The inner surfaces of the two glass windows are specified in terms of two planes $z = 0$ and $z = L$ (=25.4 cm). The flow is confined between these two planes, and is assumed to be two-dimensional; thus the field quantities - the pressure, the density, and the flow velocity, are independent of z. The interferograms were obtained using a Point Diffraction Interferometry technique[3] using a Nd:YAG laser operating at the optical wavelength 532 *nm* (see Fig. 1). The laser beam is collimated so that all the light rays passing through the flow are parallel to the z-axis. The interferogram is obtained as a sinusoidal function of the phase difference between the reference beam and the signal beam that experiences the phase modification during its passage through the flow. The reference beam here also passes through the flow and the optical imaging system but without any phase modification. Thus, the point diffraction interferometry is immune to interferogram modifications due to diffraction (Fresnel or Fraunhofer) encountered in usual holographic interferometry[4,5].

3. Ray Analysis for Optical Path Deflections in Test Flow with Large Density Gradients

As mentioned earlier, the observed fringe distortions are caused by the optical refraction induced by the large density gradient. However, the conventional treatment of the refraction (neglecting the ray deflection in the test section) is not adequate to account for the fringe distortions observed in the present experiment; thus the imaging has been more thoroughly investigated by using an analysis that includes ray deflection in the test section. In doing so, we consider a simple flow in which the air density in the test section varies only in the y-direction (see Fig. 2 for coordinates). In reality, the air density varies in the x-direction as well as in the y-direction. The analysis can be easily applied to this problem by replacing the y-coordinate variable with a one-dimensional coordinate variable which is perpendicular to the z-axis. The new coordinate axis is in the direction of $\vec{\nabla}\rho$, in a cylindrical region within which a ray under investigation is confined. In the two-dimensional flow as in the

present study, the cylinder is parallel to the z-axis.

The density variation causes variation of the refractive index in accordance with the *Gladstone-Dale* equation,[6]

$$n(y) = 1 + K\rho(y). \tag{1}$$

where K is the *Gladstone-Dale* constant whose value is .227 cm^3/g for the optical wavelength of 532 nm.

All the rays entering the test section are in the z-direction. In a flow with the density varying as in Eq. (1), a ray will be independent of x, and will stay in a y-z plane reducing the problem to two-dimensions. With reference to Fig. 2 for the coordinates (y,z), a ray in the flow is then governed by the equations that are readily derived from the eikonal equation[7]

$$\frac{d}{ds}\left(n\frac{dz}{ds}\right) = \frac{dn}{dz} = 0, \tag{2}$$

$$\frac{d}{ds}\left(n\frac{dy}{ds}\right) = \frac{dn}{dy}, \tag{3}$$

where s is a one-dimensional spatial coordinate variable along ray path.

The ray direction is specified in terms of the direction cosines dy/ds and dz/ds, which satisfy

$$\left(\frac{dy}{ds}\right)^2 + \left(\frac{dz}{ds}\right)^2 = 1, \tag{4}$$

with $dx/ds = 0$. Eq. (2) is integrated as

$$\frac{dz}{ds} = \frac{C}{n}, \tag{5}$$

with C being the integration constant to be determined. All the rays entering the test section are in the z-direction, and thus

$$\left.\frac{dz}{ds}\right|_{z=0} = 1. \tag{6}$$

It follows then that $C = n(y_0)$, y_0 being the y-coordinate of the ray entering the test section, and then Eq. (5) is written as

$$\frac{dz}{ds} = \frac{n(y_0)}{n(y)}, \tag{5'}$$

From Eqs. (5') and (4), one obtains

$$\frac{dy}{ds} = \sqrt{1 - \left(\frac{n(y_0)}{n(y)}\right)^2}. \tag{7}$$

Division of Eq. (5') by Eq. (7) yields

$$\frac{dz}{dy} = \frac{1}{\sqrt{\left(\frac{n(y)}{n(y_0)}\right)^2 - 1}}. \tag{8}$$

Integration from the ray entrance point ($y = y_0$, $z = 0$) to a point (y,z) on the ray path in the test section can be written as

$$z = \int_{y_0}^{y} \frac{dy}{\sqrt{\left(\frac{n(y)}{n(y_0)}\right)^2 - 1}}. \tag{9}$$

The refractive index of air is a function of y only, as given in Eq. (1). The air density is $0.001226\, g/cm^3$ under ambient conditions, and thus the term containing the air density, $K\rho$, is close to 0.000278, and Eq. (9) can be, to first order approximation, written as

$$z \cong \int_{y_0}^{y} \frac{dy}{\sqrt{2K(\rho(y) - \rho(y_0))}}. \tag{10}$$

This equation will be solved for a mathematical model characteristically representing a real flow subjected to a large density gradient, and solutions will be examined to account for interferogram distortions.

In the interferograms being analyzed in this study, a large interferogram distortion appears primarily in the vicinity of the upper surface of the airfoil near the leading edge for conditions of high levels of positive lift. In such a flow, the air density is the smallest on the surface, increases with increasing distance away from the surface, and then asymptotically reaches the free stream density ρ_∞. The density gradient is positive and the greatest on the surface, and decreases with increasing y. The largest ray deflection occurs near the airfoil surface (y=0). On the other hand, ray deflections are expected to be small for a short travel time in the flow. In other words, the y-coordinate variation of a ray will be small. Under these conditions, the density can be expanded as

$$\rho(y) = \rho_s + a\,y - b\,y^2 + \cdots, \tag{11}$$

where ρ_s is the density on the airfoil surface, and

$$a = \left.\frac{d\rho}{dy}\right|_{y=0}, \tag{12}$$

$$b = -\frac{1}{2}\left.\frac{d^2\rho}{dy^2}\right|_{y=0}. \tag{13}$$

In such a flow as described above, a and b are both greater than 0.

With Eq. (11) inserted into Eq. (10), the integration yields

$$y = y_0 + w\,[1 - \cos(\beta z)], \quad for\ 0 \le z \le L, \tag{14}$$

where

$$w = \frac{a}{2b} - y_0, \tag{15}$$

$$\beta = \sqrt{2Kb}. \tag{16}$$

The tangential slope of the ray is obtained as the derivative

$$y' = w\beta \sin(\beta z), \quad for\ 0 \leq z \leq L. \tag{17}$$

Once a ray exits the test section, it will follow a straight line, and is specified by a linear equation which is determined by the y-coordinate, y_L, and the slope, y'_L, of the ray at exit (z=L) of the test section. These parameters are obtained by inserting z=L respectively into Eqs. (14) and (17) as

$$y_L = y_0 + w\,[1 - \cos(\beta L)], \tag{18}$$

and

$$y'_L = w\beta \sin(\beta L). \tag{19}$$

The equation for the straight ray is then

$$y = y'_L\,(z - L) + y_L. \tag{20}$$

As governed by this equation and Eq. (14), rays are displayed in Fig. 2. As can be seen readily from Eqs. (14) and (15), the in-flow ray deflection is the greatest for the incident ray of $y_0 = 0$, and decreases with increasing y_0. From Eqs. (15) and (17), the ray slope at z=L is also seen to be the greatest for $y_0 = 0$, and to decrease with increasing y_0.

4. Image Displacement

Eq. (20) will now be examined to study imaging. When the image is focused on an object plane (z=constant), an incident ray of $y = y_0$ will constitute an image of the object that is on the ray path but will appear virtually to be located at (y,z) with y being determined by Eq. (20). Without the density variation, the ray would not deflect in the flow (as assumed in deflection-free interferometry), and would remain as a straight line parallel to the z-axis. Such a ray would be governed by the equation

$$y = y_0. \tag{21}$$

Defining the virtual displacement, δ, as the difference between Eqs. (20) and (21), one obtains

$$\begin{aligned}\delta(z) &= y'_L\,(z - L) + y_L - y_0 \\ &= w\beta \sin(\beta L)(z - L) + \\ &\qquad w\,[1 - \cos(\beta L)].\end{aligned} \tag{22}$$

For $\beta L < 1$,

$$\delta(z) \cong (a - 2by_0)KL(z - \frac{L}{2}). \tag{22a}$$

Projected onto the image plane, this virtual displacement is translated as an image displacement, $\tilde{\delta}$, which is obtained as

$$\tilde{\delta}(z) = m(z)\delta(z). \tag{23}$$

Here m is the magnification, which depends on the location of the object plane (z).

We digress here to briefly review the image formation by a spherical mirror, in terms of three parameters: f, the focal length of the mirror, and p and q, the distances from the mirror respectively to the object plane and the image plane. These parameters are interdependent through the mirror formula

$$\frac{1}{p} + \frac{1}{q} = \frac{1}{f}, \tag{24}$$

and the magnification is given by

$$m = \frac{q}{p}. \tag{25}$$

It follows that, with an image plane chosen, the location of the object plane is determined, and vice versa.

The virtual displacements on the object plane and their projection on the corresponding image planes are shown in Fig. 3. In the figure, the focal length is 10 in a relative scale used for distances. The subscripts 0 and L are used to indicate respectively the object planes z=0 and z=L. When focused on the entrance plane (z=0), p_0=19 and q_0=21.1; and focused on the exit plane (z=L), p_L=15 and q_L=30. For the incident ray with y_0=0, the virtual displacements are shown as δ_0 and δ_L on the respective object planes, and their projections on the image planes are $\tilde{\delta}_0$ and $\tilde{\delta}_L$. Note that, as evaluated from Eq. (22), $\delta_0 < 0$ and $\delta_L > 0$. As displayed in this figure, $\tilde{\delta}_0 < 0$, $\tilde{\delta}_L > 0$. It follows then that the flow image penetrates into the image of the airfoil by $-\tilde{\delta}_0$ when focused on the entrance plane z=0, as can be observed in Plate III a and b. On the other hand, when focused on the exit plane z=L, the image is separated from the the surface of the airfoil image by $\tilde{\delta}_L$, leaving the gap to be completely dark as seen in Plate IV a and b.

The analysis can be applied to a case of density variation along the surface to account for the dark spot shown near the leading edge of the airfoil as in Plate II. In this case, the y-coordinate variable is replaced by a coordinate variable parallel to the surface but perpendicular to the z-axis.

5. Quantitative Evaluation of Image Displacement for A Case of Density Variation

We now consider a density variation which is typical of dynamic stall, as displayed schematically in Fig. 3. It is mathematically modeled by the equation

$$\rho(y) = \rho_s + \Delta\rho\,(1 - e^{-y/y_e}). \tag{26}$$

Here $\Delta\rho = \rho_\infty - \rho_s$, and y_e is the y-coordinate where the air density is close to ρ_∞ with a difference of $\Delta\rho/e$.

This model exhibits the characteristics of a flow in the vicinity of a surface such as the upper surface of the airfoil near the leading edge for cases of high levels of positive lift. The air density increases with increasing y and asymptotically reaches the free stream density ρ_∞. The density gradient is the greatest on the surface and decreases with increasing y. For this flow model, one readily obtains, on inserting Eq. (26) into Eqs. (12) and (13),

$$a = \frac{\Delta\rho}{y_e}, \tag{12a}$$

$$b = \frac{1}{2}\frac{\Delta\rho}{y_e^2}. \tag{13a}$$

On inserting these into Eqs. (15) and (16), one obtains

$$w = y_e - y_0, \tag{15a}$$

$$\beta = \frac{0.0167\sqrt{\gamma}}{y_e}, \tag{16a}$$

where $\gamma = \Delta\rho/\rho_0$, and $K\rho_0 = 0.000278$ has been used.

As an example, we consider an interferogram taken with M=0.3 and α=16°. By using the fringe counting method, we determined $\gamma \cong 0.30$, and $y_e \cong 0.52cm$. For $y_0 = 0$, $w = 0.52$cm and $\beta = 0.0176$ cm^{-1}. Using Eq. (22), one obtains $\delta_L = 0.05$ cm. In this case, m=2.77; thus the image displacement $\tilde{\delta}_L = 0.14$ cm. Focused on the plane z = 0, $\delta_0 = -0.049$, m=2.22, and $\tilde{\delta}_0 = -0.11$ cm. The interferogram was taken with the system focused on three triangular objects patched on the entrance window (z=0). The fringe penetration into the airfoil image was measured from a direct comparison of the interferogram with the airfoil image taken without flow. The measurement was 0.112 cm, and is in an excellent agreement with the calculated value of $-\tilde{\delta}_0$, 0.11 cm.

6. Intensity of Deflected Light

The rays are conserved, and since the rays are almost parallel to the z-axis, the ray density is inversely proportional to the vertical separation dy of two adjacent rays. The light intensity which is proportional to the ray density is then subjected to the relation $I(y,z)dy = I_0 dy_0$, and thus

$$I(y,z) = \frac{I_0}{\frac{dy}{dy_0}}, \tag{27}$$

Here I(y,z) is the light intensity at (y,z), and I_0 is the incident light intensity at z=0, which is assumed to be uniform. From Eqs. (27) and (14), one obtains

$$I = \frac{I_0}{cos(\beta z)}. \tag{28}$$

This equation is valid only in the region specified by

$$\frac{a}{2b}[1 - cos(\beta z)] < y < a/2b. \tag{29}$$

Below the lower limit, there is no light, and the region is completely dark. As y approaches the upper limit, the expansion in Eq. (11) loses its validity. Within the valid region, Eq. (28) shows that the light intensity increases slightly with increasing z, but does not depend on y. The present analysis generates a shadowgraph as a dark spot; however, the intensity of the displaced image hardly fluctuates. This is expected because the second derivative of the air density is constant as seen from Eq. (11). The present analysis produces also schlieren effects as expected from Eq. (19). Although the deflection angle depends implicitly on y via y_0, the intensity of the schlieren images is again constant. The density variation around the airfoil is a well-behaved field; thus intensity fluctuation of shadowgraphs or of schlieren images will be minimal.

7. Concluding Remarks

Detailed understanding and correction of interferogram distortion is critical to accurate analysis of the compressible flow that occurs on airfoils at high angles of attack. Correction of these distortions is absolutely necessary if any form of flow control is to be considered in this unsteady compressible flow environment.

An analytical method was formulated to account for distortions of interferograms used in studies of dynamic stall flow. The analysis correctly predicts the distortions. However, since the method assumes a one dimensional density variation, it should be expanded and combined probably with a numerical scheme to completely correct the interferogram distortions.

Acknowledgement

We would like to express our appreciation to Dr. M. C. Wilder and Mr. J. D. Loomis for their assistance in operating the imaging system.

8. References

1. Carr, L. W., Chandrasekhara, M. S., Brock, N. J., and Ahmed, S., "A Study of Dynamic Stall using Real-Time Interferometry," AIAA 91-1007, 29th Aerospace Sciences Meeting, Reno, NV, January 7 - 10, 1991.
2. Carr, L. W., Chandrasekhara, M. S., and Brock, N. J., "A Quantitative Study of Unsteady Compressible Flow on an Oscillating Airfoil," AIAA 91-1683, 22nd Fluid Dynamics, Plasma Dynamics & Lasers Conference, Honolulu, Hawaii, June 24-26, 1991.
3. Smart, R. N., and Steel, W. H., "Theory and Application of Point-Diffraction Interferometers,"

J. Appl. Phys. Vol. 14, Suppl. 14-1, pp. 351-356, 1975

4. Goodman, J. W., *Introduction to Fourier Optics*, McGraw-Hill Book Co., San Francisco, 1968.
5. Lopez, C. A., "Diffraction Correction of Holographic Interferometric Images," AIAA 91-0564, 29th Aerospace Sciences Meeting, Reno, NV, January 7 - 10, 1991.
6. Vest, C. M., *Holographic Interferometry*, John Wiley & Sons, New york, 1979.
7. Jones, D. S., *Acoustic and Electromagnetic Waves*, Clarendon Press, Oxford, 1986.

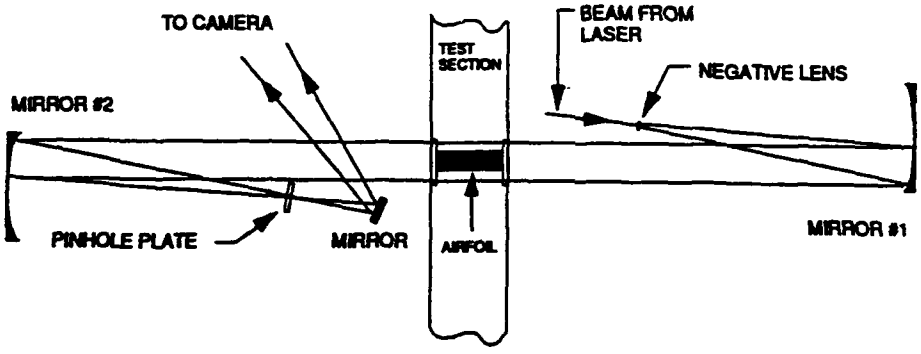

Fig. 1 Schematic of the principle of Point Diffraction Interferometry.

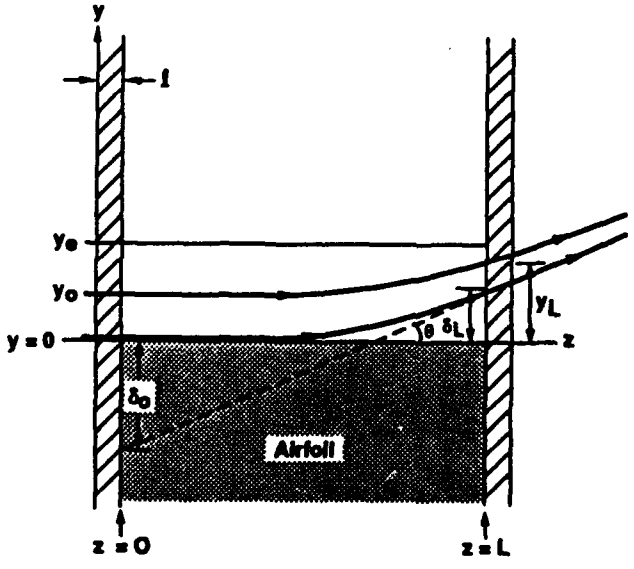

Fig. 2 Light refraction: Optical path deflection in flow.

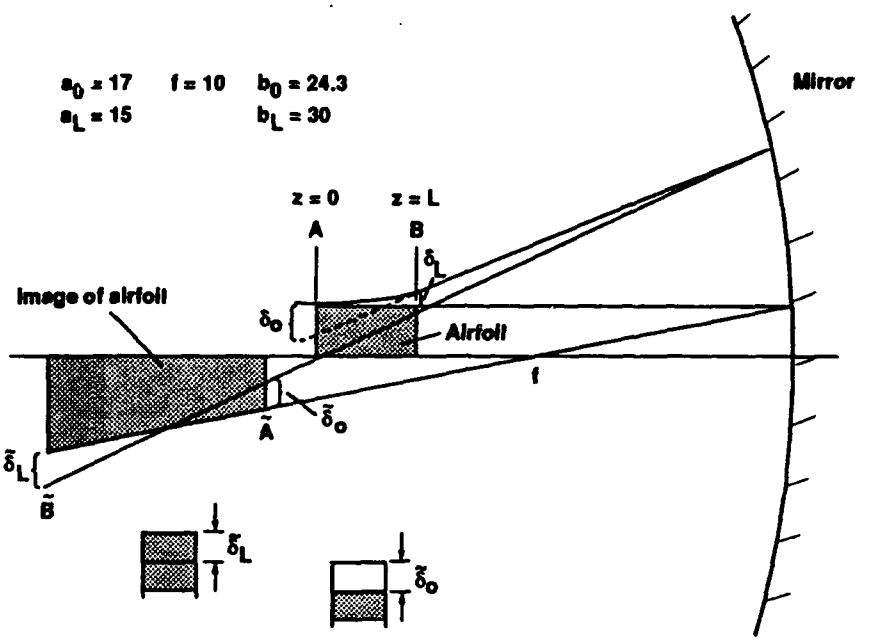

Fig. 3 Virtual and image displacements due to ray bending in flow.

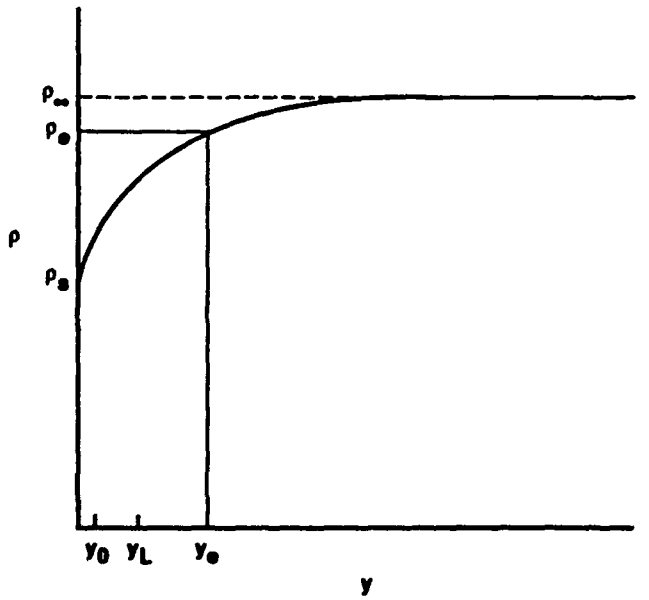

Fig. 4 Air density vs. y for a model case.

Plate I Interferogram distortion near leading edge.

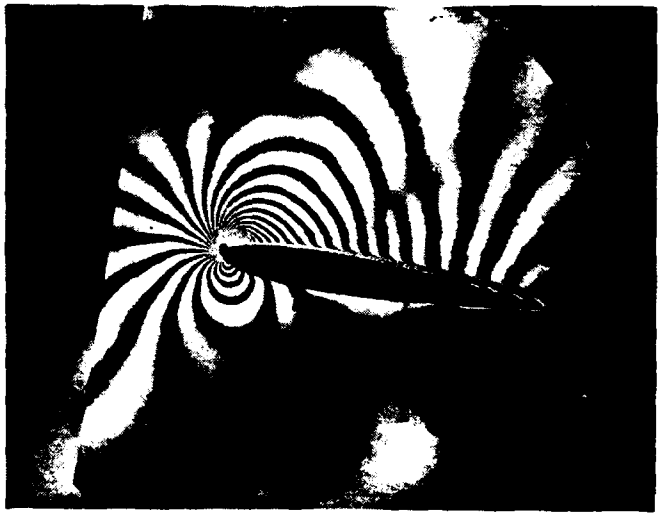

Plate II Interferogram distortion: A dark spot near leading edge.

a

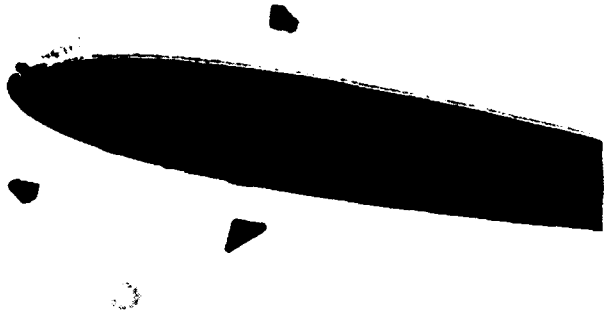

b

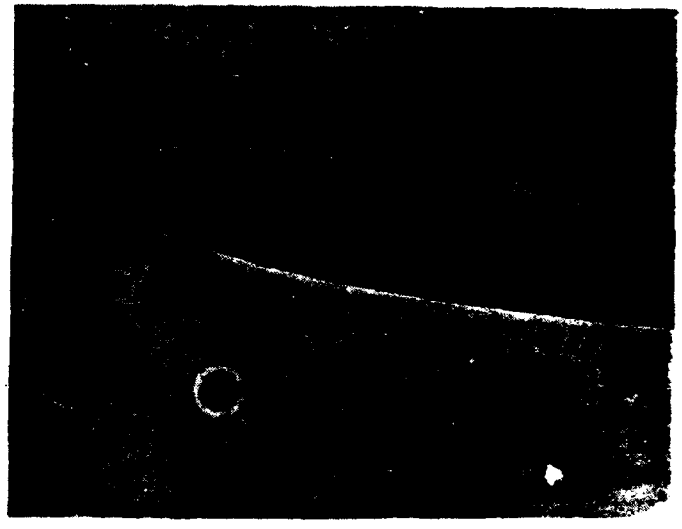

Plate III Image focused on entrance plane: α=10°; a) M=0.4, b) M=0.

a

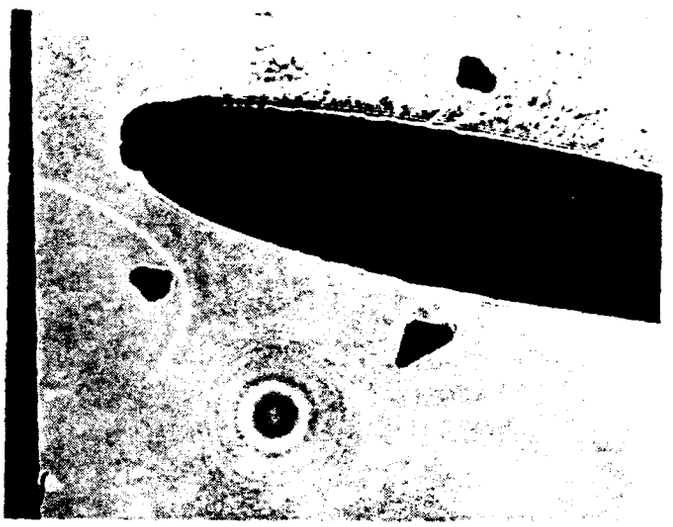

b

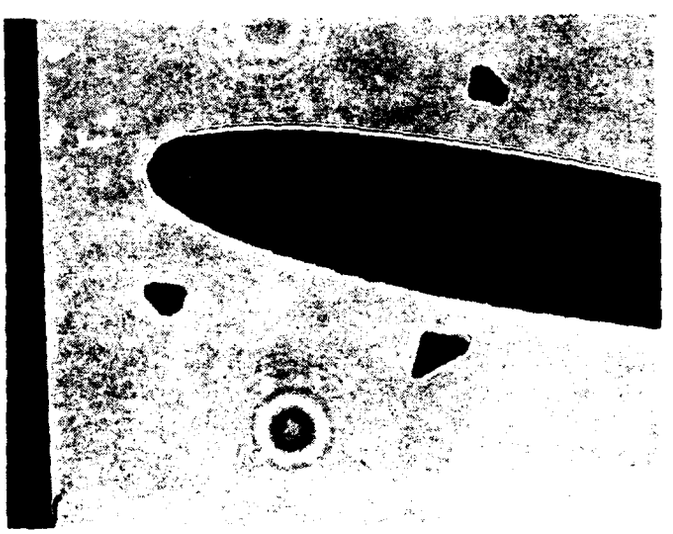

Plate IV Image focused on exit plane: α=10°; a) M=0.4, b)M=0.